COMPARISON CFD AND SYSTEM-BASED METHODS AND EFD FOR SURF-RIDING, PERIODIC MOTION, AND BROACHING OF ONR TUMBLEHOME

Hamid Sadat-Hosseini, University of Iowa, hamid-sadathosseini@uiowa.edu
Pablo Carrica, University of Iowa, pcarrica@engineering.uiowa.edu
Frederick Stern, University of Iowa, frederick-stern@uiowa.edu
Naoya Umeda, Osaka University, umeda@naoe.eng.osaka-u.ac.jp
Hirotada Hashimoto, Osaka University, h_hashi@naoe.eng.osaka-u.ac.jp
Shinya Yamamura, Osaka University, shinya_yamamura@naoe.eng.osaka-u.ac.jp
Akihiko Mastuda, National Research Institute of Fisheries Engineering, amatsuda@fra.affrc.go.jp

ABSTRACT

CFD and systems-based nonlinear dynamics approaches are used to predict broaching, surf-riding, and periodic motion for the ONR Tumblehome surface combatant, including captive and free model test validation studies. Froude-Krylov calculation of wave induced surge force in following waves provided good agreement for high Fr number, but significantly overestimated for Fr<0.2, whereas CFD successfully reproduces the decrease of the wave-induced surge force near the Fr of 0.2 probably because the CFD can capture the 3D wave pattern. CFD showed close agreement with EFD for resistance and fairly close agreement for static heel except for Y and N and static drift except for K. CFD prediction of static heel in following waves are fairly close to EFD except for X, Y and θ. System-based simulations are carried out based on inputs from EFD, CFD and Froude-Krylov for a dense grid of speed and heading and no significant changes were observed in prediction of instability map. CFD free model simulations are performed for several speeds and headings and validated for the first time for surf-riding, broaching and periodic motions.

Keywords: *Capsize, CFD, systems-based predictions, model test validation*

1. INTRODUCTION

Current research on intact stability focuses on replacing empirical criteria derived for ca. World War II mono-hull ships with dynamics-based criteria for modern merchant and naval ships. Free model wave basin experiments have identified the various capsizing modes: broaching; parametric resonance; bow diving; and pure loss of stability (Umeda and Hamamoto, 2000). Major modes are broaching and parametric roll resonance. Broaching occurs in following waves at high speed preceded by surf-riding and in quartering waves at low speed preceded by several wave encounters. Parametric resonance such as extreme amplitude parametric roll occurs in head, following and quartering waves. Bow diving occurs in following waves at high speed preceded by surf-riding on wave trough. Pure loss of stability occurs in following waves with wave crest at mid ship. Stabilized surf-riding and parametric roll or yawing is also observed. Systems-based nonlinear dynamics approaches have shown promise in predicting both broaching and parametric roll, including validation studies for conventional container, fishing, and naval ships (Umeda and Hashimoto, 2006). Such approaches require additional validation studies for unconventional

ships. Recently, CFD has for the first time shown the ability to predict stabilized parametric roll in head waves including validation studies and comparisons with systems-based nonlinear dynamics approaches (Stern and Campana, 2008) and broaching in irregular quartering waves (Carrica et al., 2008) in both cases for an unconventional naval ship, i.e., ONR tumblehome (OT). Herein, CFD and systems-based nonlinear dynamics approaches are used to predict broaching, surf-riding, and periodic motion for the OT, including captive and free model test validation studies.

2. EXPERIMENTAL METHODS

Captive model experiments were conducted for OT. Principal particulars and body plan are shown in Table 1 and Fig. 1a, respectively. The model was towed with a constant velocity. The pitch radius of gyration is different from the standard value but the effects are not large because of the low encounter frequency. Wave fixed with origin at the trough and body fixed with origin at the centre of gravity coordinate systems are used.

Most of the experiments was executed in the towing tank at Osaka University with a 1/48.94 scaled model fitted with skeg and bilge keels. A regular wave train was generated by a plunger-type wave maker. The model is free in heave and pitch, and was attached with the towing carriage via the 4 component dynamometer, which detects the surge and sway forces and the roll and yaw moments. The heave and pitch were measured by a potentiometer and a gyroscope, respectively. Calm water resistance and static heel and drift tests were conducted for Froude number Fr between 0.05 and 0.6, ϕ=(10,20) deg, and β=(2,5,10,15,20) deg. Head and following waves static heel tests were conducted for Fr between 0.1 and 0.4, ϕ=(0,10,20) deg, λ/L between 1 and 1.5, and H/L between .01 and .05. Some limited CMT tests were conducted in a conventional manner using a smaller scale OT model.

Free-running model experiments were executed with in a seakeeping and manoeuvring basin at National Research Institute of Fisheries Engineering. The basin is 60 m long, 25 m wide and 3.2 m deep. The model dimensions and its righting arm curves are shown in Table 1 and Fig. 1b, respectively. Two loading conditions were tested: one is critical to the Sarchin and Goldberg criteria and the other is slightly below them. The angles of vanishing stability under these loading conditions are 180 degrees so that capsizing cannot appear. This is because the superstructure of the OT is large. The model was propelled with two propellers. Their power was supplied from solid batteries inside the model. A feedback control system was provided to keep the propeller rate constant. The model was equipped with a fibre gyroscope, a computer and steering gears, and a proportional auto pilot for course keeping was simulated within the onboard computer by using the yaw angle obtained from the gyroscope. The roll angle, pitch angle, yaw angle, rudder angle and propeller rate were recorded by the onboard computer. Water surface elevation was also measured by a servo needle wave probe attached to the towing carriage of the basin near the wave maker.

The experimental procedure for following and quartering waves is as follows. First, the model is kept near the wave maker without propeller revolution. Next, the wave maker starts to generate regular waves. After a generated water wave train propagates enough, a radio operator suddenly requests the onboard system to increase the propeller revolution up to the specified one and makes the automatic directional control active. Then the model automatically runs in following and quartering seas to attempt to keep the specified propeller rate and auto pilot course. When the model approaches the side wall or the wave-absorbing beach, the automatic control is interrupted by the radio operator and the propeller is reversed to avoid collision. This is based on the ITTC recommended procedures on model test of intact stability 7.5-02-07-04.1. The specified

propeller rate is indicated by the nominal Fr, which is the Fr when the ship runs in otherwise calm water with that propeller rate.

In the experiment, the nominal Fr are 0.25, 0.30, 0.35, 0.40 and 0.45, the auto pilot courses, χ_c, are -5, -15, -22.5, -30, -37.5 deg from the wave direction, the wavelength to ship length ratios are 1.0, 1.25, 1.5, 1.75 and 2.0 and the wave steepness are 1/100, 1/50, 1/33.3, 1/25, 1/16.7 and 1/12.5. In total, about 200 model runs were conducted.

Two test programs were conducted as summarized in Fig. 2. Test program 1 covered GM=1.78 m and 2.068 m and χ_c, = -5, -15, and -30 deg. Difficulties were encountered maintaining constant propeller rpm, which were remedied for test program 2. Test program 2 covered GM=2.068 m and additionally χ_c, = -22.5, and -37.5 deg. The test results indicate periodic motion, surf-riding, or broaching depending on Fr and χ_c. Test program 1 indicated for GM=2.068 m: periodic motion for Fr less than or equal 0.3 and all χ_c; surf-riding for larger Fr and χ_c = -5 deg; and broaching for larger Fr and χ_c. Repeated tests are performed for six cases. Most cases show good repeatability. However, repeat tests at Fr=0.4 and χ_c = -30 deg show broaching/periodic motion and at Fr=0.45 and χ_c = -15 deg show surf-riding/broaching. For GM=1.78 m the results are similar except large Fr and χ_c show periodic motion. est program 2 boundaries differ somewhat from test program 1: periodic motion for Fr less than or equal 0.3 and all χ_c; surf-riding for larger Fr and χ_c = -5 deg; broaching then surf-riding for larger Fr and χ_c=-15 deg; and broaching for larger Fr and χ_c. Two cases of test program 2 include repeat tests and both show good repeatability. Herein, systems-based predictions are compared with results from test program 2 (Fig. 3) and CFD predictions are compared with both test programs 1 and 2.

3. SYSTEMS-BASED NONLINEAR DYNAMICS METHOD

To predict broaching associated with surf-riding of a ship having a propeller and a rudder in following and stern quartering waves, Umeda (1999) developed a system-based simulation model combining a surge-sway-yaw-roll manoeuvring mathematical model with linear wave forces calculated by a slender body theory based on a low encounter frequency assumption (Umeda et al., 1995). The hydrodynamic interactions between ship motions and waves, including the restoring variations, are ignored as higher order terms. Since the wave forces are functions of the relative ship position to waves, the mathematical model is nonlinear. Here the manoeuvring and propulsion coefficients in calm water are estimated with the conventional captive model tests.

While the above original model was validated with free-running model experiments for qualitatively identifying capsizing modes (Umeda et al., 2000), the model was upgraded with several higher order components to realise quantitative predictions with help of limited captive model experiments. (Umeda and Hashimoto, 2006) On the other hand, the original simulation model was extended to apply to a twin-screw and twin-propeller ship (Umeda et al., 2006). This model is applied to the OT.

It should be underlined here that some higher order components should be taken into account preferably with captive tests. They include i) non-linearity of wave-induced surge force, ii) non-linearity of coupling between sway and roll, iii) nonlinearity of heel-induced forces and moments in calm water. Umeda et al. (2008) and Hashimoto et al. (2008) executed the captive model experiments for these three components and reported that nonlinearity of the wave-induced surge force is not notable but forward speed effect on the wave induced surge force, which is not taken into account in the original model, is significant. Thus, this paper

focuses on the effect of the wave-induced surge force prediction method on broaching prediction. The prediction methods used for the surge force are the linear Froude-Krylov calculation, the captive model EFD and the RANS based computation CFD. The original model mentioned before uses the Froude-Krylov calculation. If the CFD can be used as an alternative to the EFD, the CFD can facilitate more practical use of a system-based simulation. Other two higher order components are estimated with captive model experiments as inputs to the system-based simulation throughout this paper.

4. CFD METHOD

CFDSHIP-IOWA v4 (Carrica et al., 2007) is a overset, block structured CFD solver designed for ship applications. Turbulence models include isotropic, non-isotropic, and DES with near-wall or wall functions. A single-phase level set method is used for free-surface capturing. Captive, semi-captive, and full 6DOF motions/forces/moments are simulated for multi-objects with parent/child hierarchy. Numerical methods include advanced iterative solvers, 2nd and higher order finite difference with conservative formulation, PISO or projection methods for the solution of pressure Poisson equation, and parallelization with MPI-based domain decomposition. Dynamic overset grids use SUGGAR.

The computational domains spans $-0.5 < x < 2$, $-1 < y < 1$, $-1 < z < 0.25$ for captive tests and $-0.6 < x < 1.8$, $-0.6 < y < 0.6$, $-0.8 < z < 0.8$ for free model tests. The ship's bow is at x = 0 and the stern at x = 1. The y axis is positive toward the starboard and the free surface at rest lies at z = 0. The ship model is appended with skeg and bilge keels for captive tests, while the free model is also appended with superstructure and twin rudders. In calm water, a coordinate system fixed to the towing tank carriage is used. Boundary conditions are applied as described in Carrica et al. (2007). For free model conditions, an Earth-fixed inertial coordinate system are used, and waves are imposed as in Carrica et al. (2008). The grid design is based on extensive use of overset grids. For free model tests, the 3.77 M points grid described in Carrica et al. (2008) is used. For test in calm water a 3.48 M points grid is used, and for captive tests in waves the grid has 3.29 M points. For the free model computations, a propeller model and an autopilot are used (Carrica et al. 2008). The propellers provide self-propulsion but in this simplified implementation the advance coefficient is computed using the total ship velocity rather than the local velocity at the propeller plane. Mimicking the experiments, a proportional controller is used as autopilot, acting on the rudders. Maximum rudder deflection and rate are also specified as given by EFD.

5. V&V POTENTIAL FLOW AND CFD METHODS FOR CAPTIVE MODEL TESTS

Potential Flow Method. The wave-induced surge force is responsible for surf-riding. Thus, it is necessary to accurately evaluate it for realising a quantitative prediction of ship behaviours in following and quartering waves. This wave-induced surge force can be calculated as the linear Froude-Krylov force as the first-order approximation, which well explains the wave-induced surge force for a small trawler up to the wave steepness of 1/10 (Umeda et al., 1995).. The measured results are compared with the Froude-Krylov calculation as shown in Fig. 1c. The wavelength to ship length ratio were 1.25 and the wave steepness were 1/50.

The comparison indicates that the linear Froude-Krylov calculation significantly overestimates the experiment when the Fr is smaller than 0.2. The Fr of 0.2 coincides with the Hanaoka parameter, $\tau = U\omega_e/g$, of 0.25 where U: the ship forward velocity, ω_e: encounter frequency and g: gravitational acceleration. Here, in an unsteady potential

flow theory with linear free-surface condition, the velocity potential relating to symmetric motions diverges. When the Hanaoka parameter increases by increasing the forward velocity, the Froude-Krylov prediction provides better agreement. The CFD successfully reproduces the decrease of the wave-induced surge force near the Fr of 0.2 probably because the CFD can capture the 3D wave pattern. The discussion with the wave pattern obtained from the CFD is the future task. As discussed with a higher-order thin ship theory by Umeda (1984), the discrepancy between the EFD and the linear Froude-Krylov calculation in higher speed region could consist of diffraction radiation and higher order Froude-Krylov components. The CFD is expected to quantitatively explain these components in the near future.

CFD Method. V&V studies have been conducted thus far for calm water resistance and static heel and drift, and static heel in head and following waves. For calm water conditions the simulations were performed using the full Fr-curve approach of Xing et al. (2008), whereby results are obtained for the full Fr range of interest in a single simulation. Single Fr simulations were conducted for some limited calm water conditions as a check and for the head and following wave conditions. Grid verification was performed for calm water static heel ϕ=10 deg using 1.22, 3.48, and 9.84 M grid points with refinement ratio $\sqrt{2}$. The medium grid was used for the initial head and following wave static heel simulations followed by simulations using an improved grid of similar total number 3.29 M, but with points redistributed for better resolution of the background waves. Validation was performed based on comparison error E = D - S for forces, moments, and motions and linear and nonlinear manoeuvring derivatives based on static heel and drift tests and wave-induced forces and moments based on static heel in following wave tests using the systems-based method mathematical model. Consideration is given to averages over Fr and ξ_g/λ based on absolute error in %D $\overline{E} = \frac{1}{N}\sum_{i=1}^{N}\left|E_i / D_i\right|$ and in %DR $\overline{E} = \frac{1}{N}\sum_{i=1}^{N}\left|E_i / DR\right|$ and RSS error in %D $\overline{E_{RSS}} = \frac{1}{N}\sqrt{\sum_{i=1}^{N}\left(E_i / D_i\right)^2}$, and maximum errors E_{max} in %D and %DR. The average RSS error seems most representative. Future work will include verification for following wave static heel conditions and similar studies for the CMT tests.

Table 2 provides the grid verification results. Y for all Fr and N/σ for large Fr show relatively poor convergence, i.e., Fr regions with oscillatory convergence or divergence. Nonetheless the overall conclusion is that the results are fairly insensitive to grid changes for present range of grid sizes. The RSS average Ug=3%S_1. Y and N show the largest Ug, which are more than 3 times larger than the average values.

Figures 4 and 5 include calm water resistance results. $\overline{E}_{RSS}$=3%D for X, σ, and τ is typical for X and smaller than typical by factor of about 3 for σ, and τ. E_{max}%D is about 3 times larger and occurs at large Fr. Figure 4 provides the calm water static heel results. Fairly close agreement is shown for σ, τ, X, K for the full Fr range, whereas Y and N are significantly under-predicted for Fr>0.4. $\overline{E}_{RSS}$ = 6-7%D for ϕ=10 and 20 deg. E_{max}%DR are about 3 times larger. Errors are similar for heel angle 10 and 20 deg. The linear and nonlinear manoeuvring derivatives $\overline{E}_{RSS}$=7 and 107%D, respectively. Figure 5 provides calm water static drift results. Fairly close agreement is shown for σ, τ, X, Y, N for the full Fr range, whereas K is over predicted for Fr>0.2. $\overline{E}_{RSS}$ = 10%D except for K for which $\overline{E}_{RSS}$ =50%D, E_{max}%DR are about 3 times larger. Errors are similar for drift angle 5, 10 and 15 deg. The linear and nonlinear manoeuvring derivatives $\overline{E}_{RSS}$ =8 and 20%D,

respectively, excluding K and $\bar{E}_{RSS}$ =30%D including K. For static heel in following waves, EFD and CFD X, Y, K, N, z, θ vs. ξ_g/λ were constructed based on averages over 2-5 wave periods and $\bar{E}_{RSS}$ evaluated, as provided in Table 3. Overall trends are predicted by CFD. For ϕ=0.0, the average error is 15%D with the largest errors for X and θ. The average error increases by factor of 2 for same increase in wave amplitude. For ϕ=10 and 20 deg, the average error is also about 15%D with the largest errors for X and Y.

6. V&V SYSTEMS-BASED AND CFD METHODS FOR FREE MODEL TESTS

Systems-Based Method. Since notable difference in the wave-induced wave surge force among the EFD, the Froude-Krylov prediction and the CFD, it is important to examine the effect on system-based prediction of ship motions including surf-riding, broaching and periodic motion. For this purpose, system-based simulation using the mathematical model mentioned before was executed for the cases of free model tests of the OT with three different wave-induced surge force estimation, i.e. the EFD, the Froude-Krylov prediction and the CFD as input data.

A systematic numerical simulation was executed for a dense grid of operational parameters with GM of 2.068 m, the wavelength to ship length ratio of 1.25 and the wave steepness of 1/20. The initial state used here is a periodic state under the nominal Fr of 0.1 and the auto pilot course of 0 degrees from the wave direction. Then the operational parameters are suddenly changed to the specified values, similar to the free-running model experiments. Based on the obtained time series, the ship motions are qualitatively categorised as periodic motion having periods equal to the encounter period, stable surf-riding and others. The result of the system-based simulation with the wave-induced surge force estimated by the Froude-Krylov calculation is shown with the experimental data in Fig. 3a (Umeda et al., 2008). When the auto pilot course is smaller, there is a boundary between the stable surf-riding and periodic motion near the nominal Fr of 0.3. Below this boundary, periodic motions are simulated as they are identified in the experiments. Above this boundary, a stable surf-riding region exists, and includes the stable surf-riding identified in the experiment. However, this region also includes the case of broaching in the experiment. When the auto pilot course is larger, the simulated roll exceeds 90 degrees above the nominal Fr of 0.3. On the other hand, in the experiment the maximum roll angle is 71 degrees. This means that the mathematical model overestimates the roll angle and underestimates the yaw deviation. It can be presumed that this is induced by the emergence of propeller and rudder out of water, which could reduce the yaw checking ability under the extreme roll angle. In the region categorised as "not identified." sub-harmonic motions often are obtained.

The result of system-based simulation using the wave-induced surge force measured in the captive model experiment is shown in Fig. 3b. Although notable discrepancy in the wave-induced surge force exists as shown in Fig. 1c, the difference in the system-based simulation results between the two is not significant. One surf-riding related broaching case in the free model test where the auto-pilot course of 22.5 degrees and the nominal Fr of 0.35 is categorized as a harmonic periodic motion in the system-based simulation with the wave-induced surge force measured in the captive model tests, while it is done as stable surf-riding in the simulation shown in Fig. 3a. This is because the wave-induced surge force is smaller in this system-based simulation.

In case of the system-based simulation using the wave-induced surge force estimated by the CFD as shown in Fig. 3c, the stable surf-riding zone further but slightly shrinks because of smaller wave-induced surge force at relevant speed. Other notable change is not found. As a

whole, for this subject ship, the Froude-Krylov calculation for estimating the wave-induced surge force is satisfactory.

CFD Method. CFD studies are performed for λ/L=1.25, H/λ=0.05, Fr=0.4, GM=2.068 m and χ_c = 5, 15 and 30 deg, and GM=1.78 m and χ_c = 15 deg for test program 1 and for λ/L=1.25, H/λ=0.05, Fr=0.3,0.35,0.4,0.45, GM=2.068 m and χ_c = 5, 15, 22.5 and 30 deg for test program 2. These cases are selected to check the ability of CFD to predict the boundary of instability shown in Fig. 2. Herein, only results for Fr=0.4 are discussed.

For each case, the initial wave phase and surge velocity are not provided by experimental data but estimated from trial and error method. Initial roll, pitch, yaw angle and rudder deflection are estimated from their experimental time histories. Self-propulsion is computed free to sink and trim in calm water, using a speed controller to reach Fr=0.4. The predicted RPS is then prescribed for the free model simulations at the same nominal Fr number. CFD self-propulsion RPS is predicted 19.57 rps to reach Fr=0.4, 5.8% higher than EFD. The resulting sinkage, trim and thrust force are 10.9 mm, 0.36 deg and 22.7 N, respectively. CFD and EFD comparisons for free model are shown in Fig. 6 to discuss CFD prediction of surf-riding, broaching, and periodic motion for test program 2 (Figs. 6a,b,c,d) and test program 1 (Figs. 6e,f,g,h). Discussions are based on additional figures for forces, moments, and trajectories.

Fig. 6a shows the case of stable surf-riding (χ= 5 deg) with initial wave phase=50 deg and surge velocity=0.2. After an initial transient in which one wave overcomes the ship, the model gets locked in waves. During the initial transient, the rudder turns the model to the desired course so that the ship travels near to right heading at t=5 s and is captured by the wave down slope causing a negative pitch angle. After that, the ship velocity equals the wave velocity and surf-riding occurs. A similar process is also observed for cases 85 (χ= 5 deg) and 169 (χ= 15 deg), as shown in Figs. 6b and 6f. Notice that in case 169 the ship is unable to maintain the target heading, deviating about 10 deg to port.

The case of broaching is shown in Fig. 6c for χ= 22.5 deg with initial wave phase=200 deg and surge velocity=0.55. In CFD predictions, the ship moves slightly slower than in EFD, probably due to inaccurate initial conditions. The pitch shows that the ship experiences surf-riding for about 6 seconds starting immediately after releasing the model. During surf-riding, the negative yaw angular velocity not only results in turning broadside to the wave but also induces a centrifugal force together with large forward velocity. This centrifugal force realises the roll angle of +50 deg. Based on CFD calculation of action (wave-induced) and reaction (rudder- and propeller-induced) moments, not shown here, the wave induced yaw moment is such that at t=5 s (N_h=-100 N.m) is much stronger than any other moments (essentially the rudder moment) trying to counteract it, and causes broaching. The broaching continues up to t= 7 s, when the heading is about 70 deg. At this point, the wave induced yaw moment reaches 100 N.m helping the ship to turn toward the target direction and recover. During the broaching process, the effects of propeller moments on broaching, as predicted by the simplified body force model, are negligible. The propeller yaw moment is 10 times smaller than the rudder yaw moment. In fact, the propeller yaw moment should be zero due to the symmetric behaviour of the model for twin counter-rotating propellers. However, one of two propellers emerges out of water temporally resulting in non-zero roll and yaw moments. This might cause loss of control even though it cannot be the main reason for broaching. The same procedure of broaching is observed for cases 41 and 84 with χ= 15 deg as shown in Figs. 6e and 6g.

Fig. 6d shows the case of periodic motion with χ_c = 30 deg, initial wave phase=144 deg and surge velocity=0.2. The yaw angle shows that the model is released at -20 deg heading

respect to the target. At t=3 s, when the ship is at the target heading, the wave induced yaw moment (N_h=-100 N.m) overwhelms the rudder reaction moment (N_R= 10 N.m) causing the vessel to turn hard to 30 degrees respect to the target at t= 5 s. At this time, the rudder yaw moment is positive and large enough to turn the ship toward target heading but overshooting 10 deg at t=6.5 s. At this time again the wave yaw moment is stronger than the rudder reaction and the ship turns back to 30 deg heading respect to the target, with the process repeating resulting in a periodic motion. A similar process is observed for case 83 as shown in Fig. 6h.

7. CONCLUSIONS AND FUTURE RESEARCH

CFD and systems-based nonlinear dynamics approaches are used to predict broaching, surf-riding, and periodic motion for the ONR Tumblehome surface combatant, including captive and free model test validation studies.

Froude-Krylov calculation of wave induced surge force in following waves provide good agreement for high Fr number, but significantly overestimate for Fr<0.2. The CFD successfully reproduces the decrease of the wave-induced surge force near Fr=0.2 probably because the CFD can capture the 3D wave pattern.

The grid study for calm water static heel indicates that the average RSS grid uncertainty is $\bar{E}_{RSS}$ =3%D. CFD resistance in calm water shows close agreement with EFD with average RSS error of 3%D for X, σ, τ. CFD and EFD static heel results show fairly close agreement for σ, τ, X, K for the full Fr range, whereas CFD Y and N are significantly under-predicted for Fr>0.4. CFD static drift shows good results of σ, τ, X, Y, N for the full Fr range, whereas K is over-predicted for Fr>0.2. CFD shows fairly close agreement for static heel and drift linear manoeuvring derivatives, whereas large errors are indicated for nonlinear manoeuvring derivatives especially for static heel. CFD static heel in following waves average errors are $\bar{E}_{RSS} = 15\%D$ with the largest errors for surge and sway forces and pitch motion.

System-based simulations based on inputs from EFD, CFD and Froude-Krylov calculation are performed for a dense grid of speeds and headings. No significant changes in instability map are observed using Froude-Krylov calculation or CFD as replacements for EFD. When the auto pilot course is less than 20 deg, there is a boundary between surf-riding and periodic motion near the nominal Froude number Fr=0.3. Periodic motion/surf-riding are observed below/above this boundary. There are differences between EFD and system-based prediction at Fr>0.3 and χ>30 deg in that simulated roll exceeds 90 degrees while experiment tops at 71 deg. This discrepancy can be probably fixed by adding effects of emergence of propeller and rudder out of water to the model.

CFD free model simulations show promising results for surf-riding, broaching and periodic motion. CFD calculation of wave and heel induced yaw moments and rudders yaw moment help explain the processes of surf-riding, broaching, and periodic motion. It is concluded that wave and heel induced yaw moments are the major causes of broaching/periodic motion, with rudder and propeller moments much smaller in magnitude. The results show a phase difference between CFD and EFD, possibly due to inaccurate initial conditions and/or propeller modelling.

Future work in CFD captive computations includes verification for following wave static heel conditions, more complete validation focusing on the systems-based method mathematical model, and similar studies for CMT tests. This would check the reliability of CFD as a surrogate of captive experiments for system based simulations. For CFD free model simulations, more cases will be run and more analysis will be carried out to understand the dynamics of different capsize modes. The

accuracy of CFD free model simulations will be improved by adding a discretized rotating propeller to the CFD grid instead of using body force propeller model. It is expected that the CFD and EFD agreement will be improved even though the role of the uncertainty on initial condition would be still an issue.

8. ACKNOWLEDMENTS

Sponsored by ONR grant N00014-01-1-0073 and NICOP contract N00014-06-1-0646 under administration Dr. Patrick Purtell, and Grant-in Aid for Scientific Research from the Japan Society for Promotion of Science (No. 18360415).

9. REFERENCES

Carrica, P.M., Wilson, R., Noack, R., and Stern, F., 2007, "Ship Motions using Single-Phase Level Set with Dynamic Overset Grids, Computers & Fluids, Vol. 36, pp. 1415-1433.

Carrica, P.M., Paik, K.J., Hosseini, H.S. and Stern, F. 2008, "URANS analysis of a broaching event in irregular quartering seas," Journal of Marine Science and Technology, Vol.13, pp.395-407.

Hashimoto, H., Stern, F., Sadat-Hosseini, S., and Sueyoshi, M., 2008, "An Application of CFD to Recent Ship Stability Problems", Proceedings of the 10th International Ship Stability Workshop, Daejeon, pp.23-30.

Stern, F. and Campana, E., 2008, "Head-Waves Parametric Rolling of Surface Combatant," Proceedings of the Symposium on Limit Cycle Oscillation and Other Amplitude-Limited Self-Excited Vibrations, AVT-152, Loen, Norway.

Umeda, N. and M. Hamamoto, 2000, "Capsize of Ship Models in Following/ Quartering Waves –Physical Experiments and Nonlinear Dynamics-", Philosophical Transactions of the Royal Society of London, Series A, Vol. 358, pp.1883-1904.

Umeda, N. and Hashimoto, H., 2006, "Recent Developments of Capsizing Prediction Techniques of Intact Ship Running in Waves", Proceedings of the 26th ONR Symposium on Naval Hydrodynamics, Rome, CD.

Umeda, N., 1999, Nonlinear Dynamics on Ship Capsizing due to Broaching in Following and Quartering Seas, Journal of Marine Science of Technology, Vol.4, pp.16-26.

Umeda, N., Maki, A. and Hashimoto, H. 2006, "Manoeuvring and Control of a High-Speed Slender Vessel with Twin Screws and Twin Rudders in Following and Quartering Seas"Journal of the Japan Society of Naval Architects and Ocean Engineers, Vol. 4, pp.155-164, (in Japanese).

Umeda, N., Yamakoshi, Y. and Suzuki, S., 1995, "Experimental Study for Wave Forces on a Ship Running in Quartering Seas with Very Low Encounter Frequency", Proceedings of the International Symposium on Ship Safety in a Seaway, 14.1-18.

Umeda, N., Munif, A. and Hashimoto, H., 2000, "Numerical Prediction of Extreme Motions and Capsizing for Intact Ships in Following / Quartering Seas", Proceedings of the 4th Osaka Colloquium on Seakeeping Performance of Ships, Osaka, pp.368-373.

Umeda, N., Yamamura, S., Matsuda, A., Maki, A., Hashimoto, H., 2008, "Model Experiments on Extreme Motions of a Wave-Piercing Tumblehome Vessel in Following and Quartering Waves", Journal of the Society of Naval Architects and Ocean Engineers of Japan, Vol. 8, pp.179-185.

Umeda,N., 1984, Resistance Variation and Surf-riding of a Fishing Boat in Following

Sea, Bulletin of National Research Institute of Fisheries Engineering, No.5, pp.185-205.

Xing, T., Carrica, P., and Stern, F., 2008, "Computational Towing Tank Procedures for Single Run Curves of Resistance and Propulsion," ASME J. Fluids Eng.

Table 1. Principal particulars of the ONR tumblehome model used in the captive and free-running model experiments.

Items	*Ship*	*Model*	*Items*	*Ship*	*Model*
Length : L	154.0 m	3.147 m	Metacentric height : GM	i)1.781 m ii) 2.068 m	i) 0.0364 m ii) 0.0423 m
Breadth : B	18.78 m	0.384 m			
Depth : D	14.5 m	0.296 m	Natural roll period : T_φ	i) 12.38 s ii) 11.68 s	i) 1.77 s ii) 1.67 s
Draught : d	5.494 m	0.112 m			
Displacement : W	8507 ton	72.6 kg	Radius of gyaration in pitch : K_{yy}/L	i) 0.25 ii) 0.25	i) 0.254 ii) 0.246
Block coefficient : C_b	0.535	0.535			
Longitudinal position of centre of buoyancy from midship : LCB	2.587 m aft	0.053 m aft	Rudder area : A_R	28.639 □ ×2	0.012 □ ×2
Maximum rudder angle: δ_{MAX}	±35°	±35°			

Table 2. Grid verification results.

Refinement ratio=!2	**X**	**Y**	**K**	**N**	**σ**	**τ**
DR	51.83 (N)	5.44 (N)	4.18 (N.m)	10.20 (N.m)	12.95 (mm)	1.65 (deg)
Ug(%D)	1.32	25.92	1.35	20.96	3.23	5.80
Ug(%DR)	0.42	6.57	1.31	5.48	1.55	1.18
Ug (%D); RSS	0.10	6.75	1.02	5.11	2.29	2.36

Table 3. Summary of following waves results.

Heel&Fr	**Wave**	**X**	**Y**	**K**	**N**	**z**	**θ**	$\overline{E}$
Heel10-Fr=0.3	H/λ=0.03;λ/L=1	35.29011	45.02286	3.93254	6.67891	8.35731	4.87985	16.85
Heel20-Fr=0.3	H/λ=0.03;λ/L=1	27.05689	23.62012	3.38126	3.28103	8.80345	6.56903	12.11
Heel0-Fr=0.35	H/λ=0.025;λ/L=1.25	9.98453				4.69035	30.7823	15.15
Heel0-Fr=0.35	H/λ=0.05;λ/L=1.25	18.54791				9.49351	58.0826	28.70

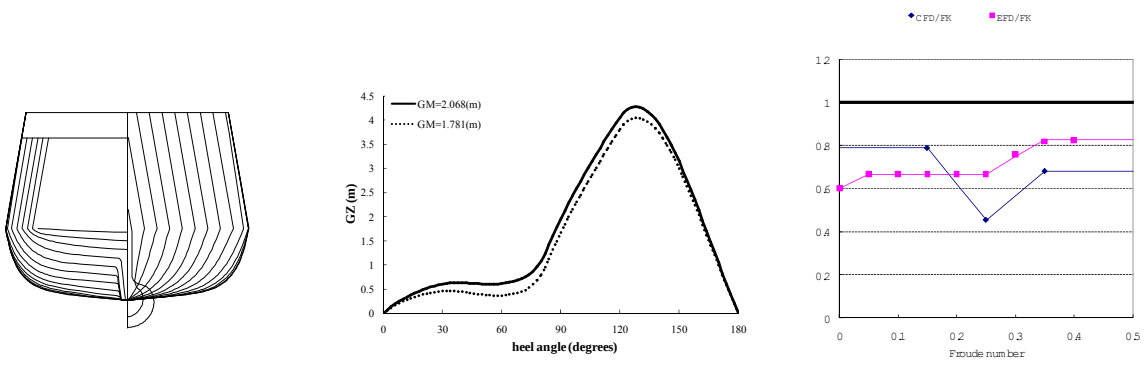

(a) (b) (c)

Figure 1. ONR Tumblehome vessel: (a) Body plan; (b) GZ curve; (c) EFD, CFD, and Froude Krylov cal. of wave-induced X force for λ/L=1.25 and H/λ =0.025.

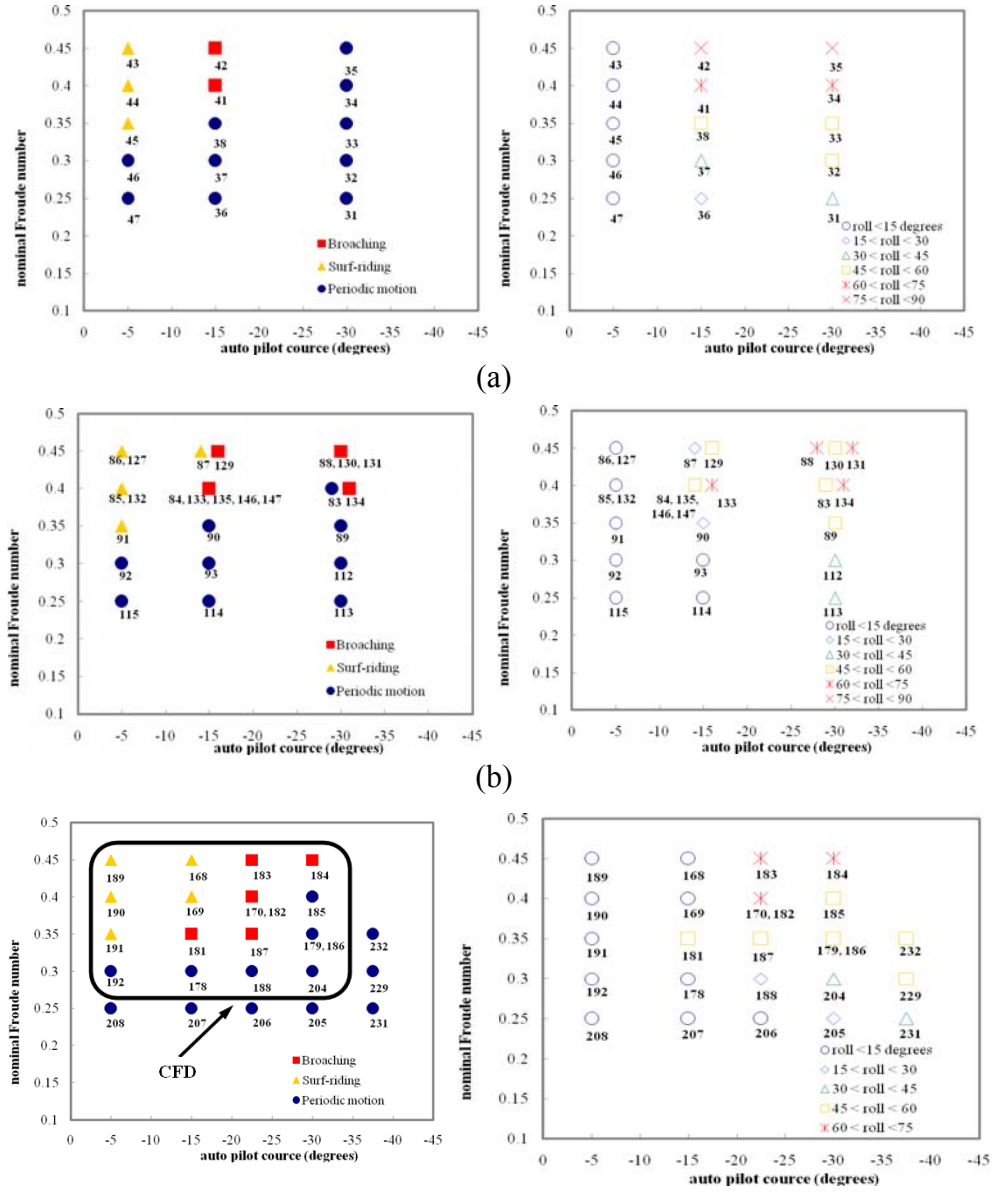

Figure 2. Summary of free model test program 1 and 2: (a) test program 1 and GM=1.78 m, (b) test program 1 and GM=2.068 m, (c) test program 2 and GM=2.068 m.

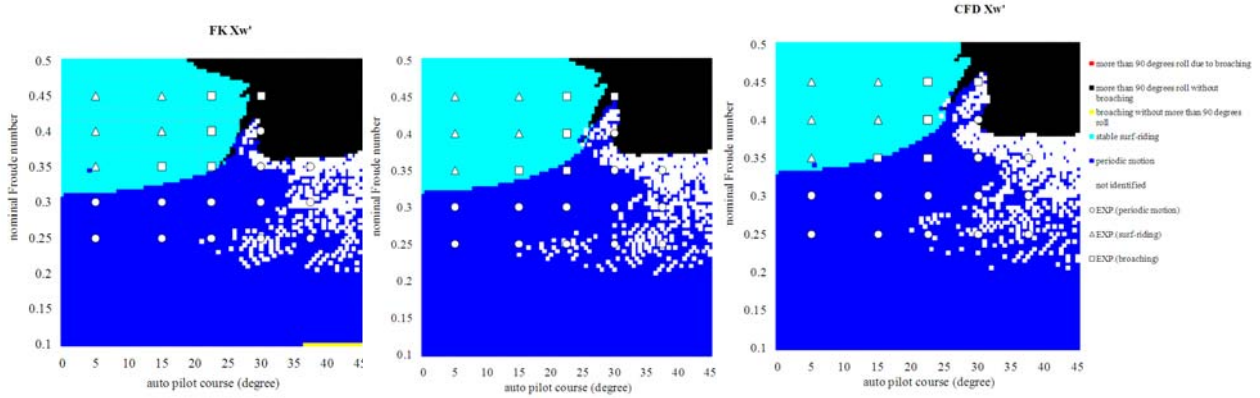

Figure 3. Comparison between the free model test and the system-based numerical simulation for GM=2.068m, H/λ=1/20 and λ/L=1.25 using the wave-induced surge force estimated by: (a) the Froude-Krylov prediction (Umeda et al., 2008); (b) captive model experiment; (c) CFD.

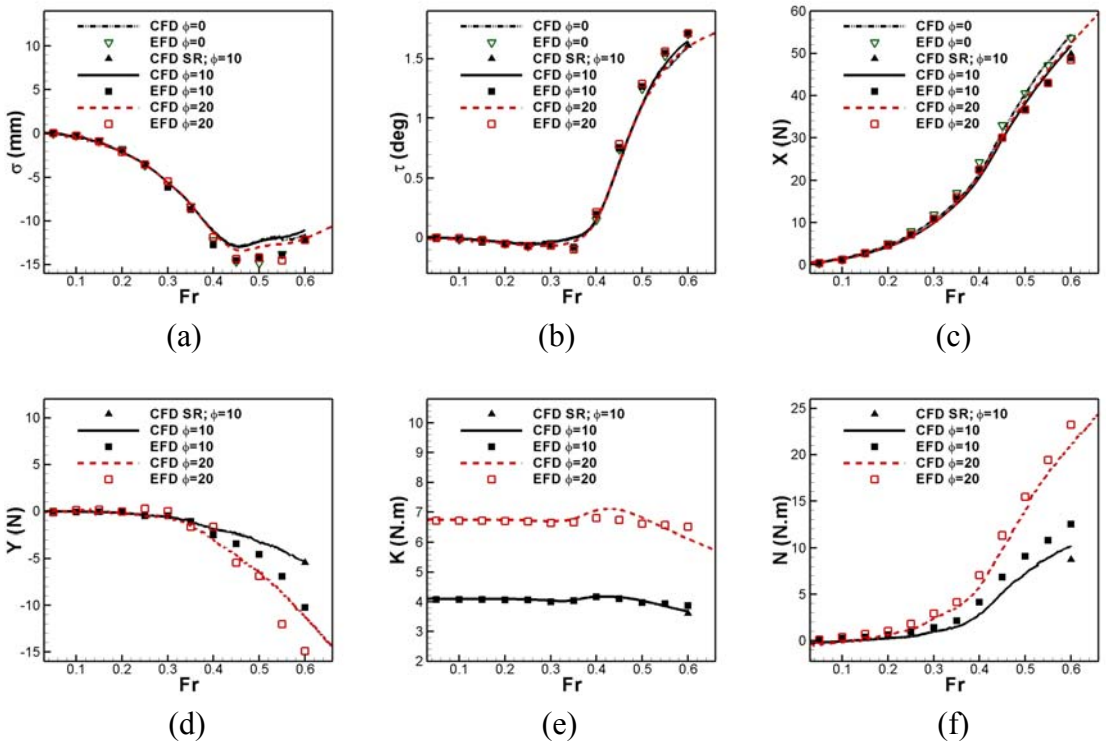

Figure 4. Static heel CFD and EFD comparison of: (a) sinkage, (b) trim, (c) axial force, (d) side force, (e) roll moment, (f) yaw moment.

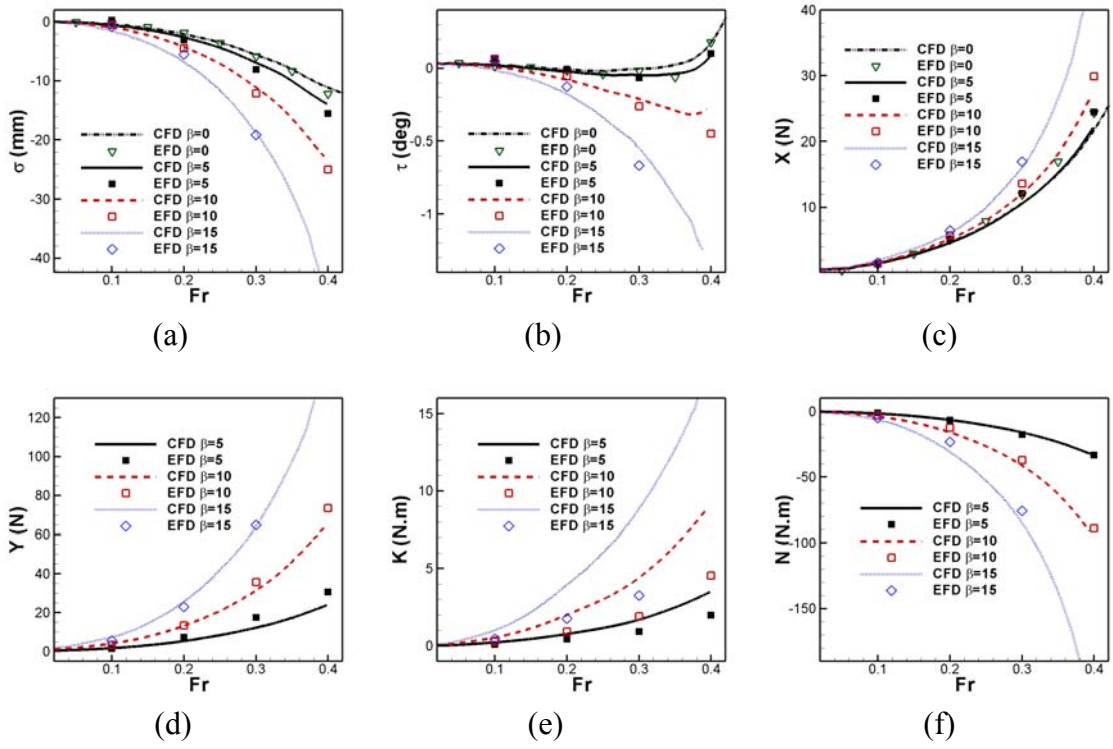

Figure 5. Static drift CFD and EFD comparison of: (a) sinkage, (b) trim, (c) axial force, (d) side force, (e) roll moment, (f) yaw moment.

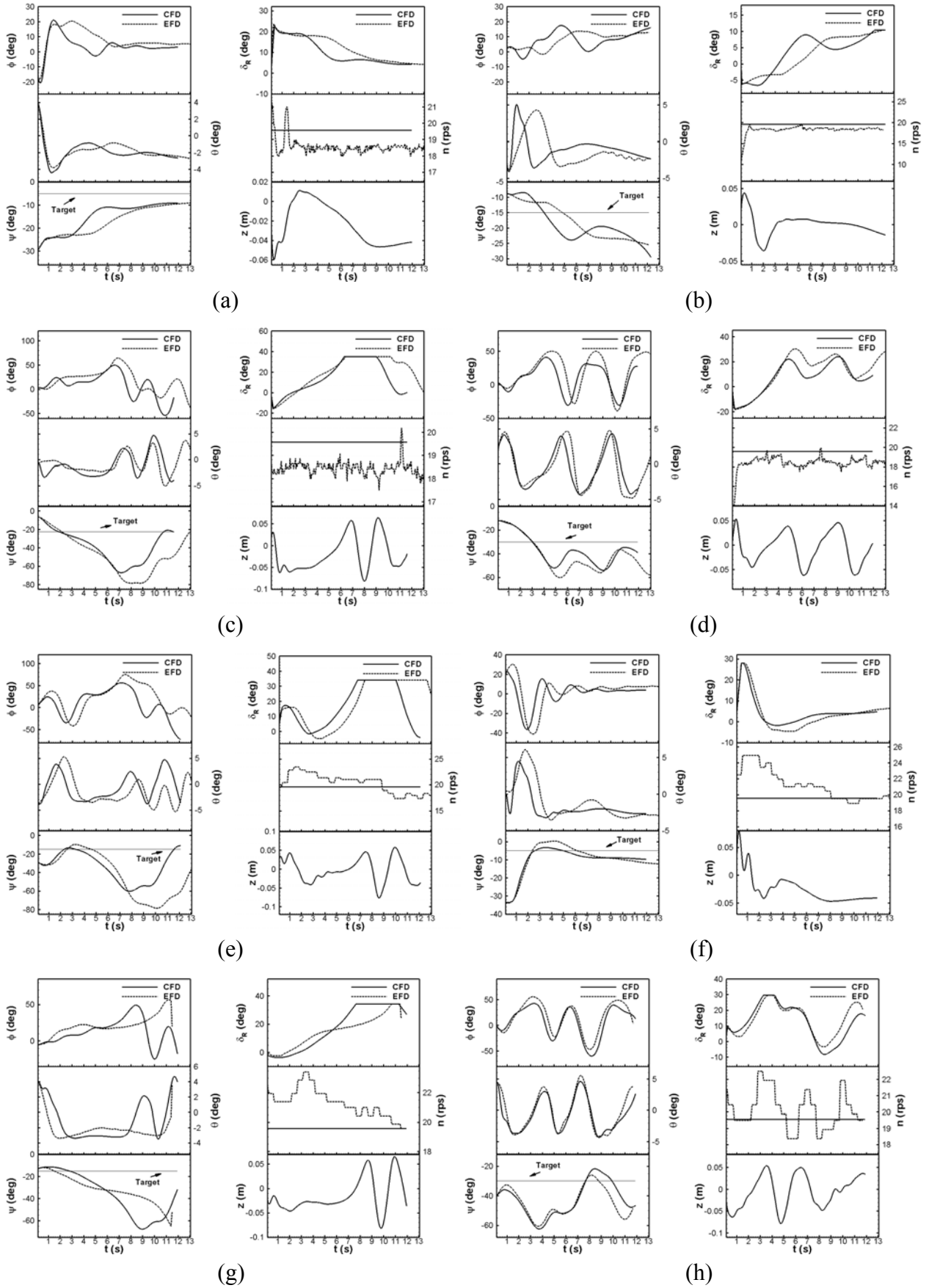

Figure 6. CFD and EFD for case number: (a)190, (b)169, (c)170, (d)185, (e)41, (f)85, (g)84, (h)83.